Uptake-leak balance of SR Ca^{2+} determines arrhythmogenic potential of $RyR2^{R420Q+/-}$ cardiomyocytes

Ruben Lopez [a], Radoslav Janicek [a], Miguel Fernandez-Tenorio [a], Marianne Courtehoux [a], Lluis Matas [a], Pascale Gerbaud [b], Ana M. Gomez [b], Marcel Egger [a], Ernst Niggli [a,*]

[a] *Department of Physiology, University of Bern, Bern, Switzerland*
[b] *INSERM UMR-S 1180, Université Paris Saclay, Châtenay-Malabry, France*

ARTICLE INFO

ABSTRACT

Mutations of the RyR2 are channelopathies that can predispose to life threatening catecholaminergic polymorphic ventricular tachycardias (CPVTs) during exercise or stress. However, the cellular and molecular mechanisms that are causal for the arrhythmias downstream of the β-adrenergic receptor (β-AR) activation are not defined. They may be specific and different for each particular RyR2 mutation. Obvious possibilities are the phosphorylation of the mutated RyR2s or the stimulation of the SR Ca^{2+} pump (SERCA), which could increase SR Ca^{2+} loading. Potentially arrhythmogenic Ca^{2+} signals, such as Ca^{2+} waves, were recorded and analyzed from WT and $RyR2^{R420Q+/-}$ mouse cardiomyocytes with confocal microscopy after field stimulation at 1 Hz. In $RyR2^{R420Q+/-}$ cardiomyocytes we found a higher occurrence and frequency of Ca^{2+} waves, particularly upon β-AR stimulation with isoproterenol. This was accompanied by a shorter latency to the first spontaneous wave. Wave velocity from raw traces, as well as amplitude and decay time constant (τ) analyzed in de-skewed traces were comparable in both cell types. To obtain further insight into the role of the SERCA we selectively stimulated SERCA in permeabilized myocytes using Fab fragments of a PLB antibody (2D12). Surprisingly, SERCA stimulation alone resulted in considerably higher wave frequencies than when mimicking β-AR stimulation with cAMP, particularly in $RyR2^{R420Q+/-}$ cardiomyocytes. This may be a consequence of some protective SR Ca^{2+} unloading resulting from the SR Ca^{2+} leak via phosphorylated RyR2s in cAMP. Spark-to-spark recovery analysis suggested a remarkably higher Ca^{2+} release sensitivity in $RyR2^{R420Q+/-}$ cells, both in control and upon β-AR stimulation. Together these findings suggest that the fine balance between SR Ca^{2+} loading via SERCA and the Ca^{2+} leak via mutated and phosphorylated RyR2s is an important determinant for the overall cellular arrhythmogenicity prevailing in the $RyR2^{R420Q+/-}$ myocytes.

1. Introduction

In cardiac muscle of most species, the Ca^{2+} signals controlling the strength of contraction from beat to beat are largely governed by Ca^{2+} release from the sarcoplasmic reticulum (SR). This transient Ca^{2+} release occurs by the Ca^{2+}-induced Ca^{2+} release (CICR) mechanism via tetrameric ryanodine receptor channels type 2 (RyR2s in cardiac muscle) located in the SR membrane (for review see [1]). RyR2s normally have a very low open probability (P_o) at resting cytosolic Ca^{2+} concentrations (i.e. at the time of the diastole). During each action potential the P_o of the RyR2 is substantially increased by Ca^{2+} entering via L-type Ca^{2+} channels. Between beats, the low yet non-zero RyR2 P_o gives rise to accidental but highly localized SR Ca^{2+} release signals, termed "spontaneous Ca^{2+} sparks".

While individual spontaneous Ca^{2+} sparks do not affect the electrophysiology of the cardiomyocytes, they may aggregate into Ca^{2+} waves under pathological conditions. Ca^{2+} waves traveling along the cell may initiate delayed after depolarizations (DADs) of the membrane, which in turn can form a substrate for arrhythmias.

A number of mutations of the RyR2s have been identified [2,3]. Most of these mutations result in a gain-of-function on the level of the RyR2 channel [4–6], a few confer a loss of function [7,8]. Interestingly, and

apparently irrespective of the change in molecular function, many of the known RyR2 mutations precipitate similar clinical pictures with arrhythmias in structurally normal hearts. These arrhythmias often manifest themselves as potentially live threatening catecholaminergic polymorphic ventricular tachycardias (CPVTs) prompted by physical exercise or emotional stress.

Given the diversity of observed RyR2 mutations, the cellular mechanisms linking the molecular dysfunction of the RyR2s to the resulting arrhythmogenic events on the cellular and organ level are most likely quite diverse, depending on the mutated residue on the RyR2. This would imply that distinct pharmacological approaches may be optimal to treat each particular mutation (or group of mutations with similar ramifications on the molecular level). Understanding these arrhythmias on the molecular, cellular and organ level may therefore open the door for personalized treatment options.

Since during physical exercise or emotional stress the ß-adrenergic receptor (ß-AR) signaling affects a range of proteins involved in Ca^{2+} signaling and excitation-contraction coupling (EC-coupling) of cardiac myocytes, several subcellular mechanisms could be responsible for actually triggering the arrhythmia. An obvious possibility how the arrhythmia could be precipitated is via phosphorylation of the RyR2s, which may further increase the abnormal Ca^{2+} sensitivity of the mutated channels thereby increasing the SR Ca^{2+} leak [9–11]. In addition, during β-AR activation a stimulation of the SERCA will also occur after phosphorylation of phospholamban (PLB). This SERCA stimulation in turn will accelerate the rate of SR refilling and may increase the SR Ca^{2+} load, which by itself is also known to be arrhythmogenic [12].

In the present study we examined the role of both, RyR2 phosphorylation and SERCA stimulation during β-AR stimulation in cardiomyocytes isolated from a mouse model of a gain-of-function CPVT mutation, RyR2$^{R420Q+/−}$ [13,14]. The results suggest that both RyR2 phosphorylation but also SERCA stimulation can contribute to the generation of arrhythmogenic signals, such as Ca^{2+} waves. Interestingly, both mechanisms can either contribute additively or negatively to the overall arrhythmogenicity. The RyR2 phosphorylation increases the SR Ca^{2+} leak, and thereby also unloads the SR from Ca^{2+}. The SERCA stimulation favors the generation of Ca^{2+} waves by loading the SR with Ca^{2+}, but also reduces the cytosolic Ca^{2+} concentration, thereby increasing the threshold for wave propensity [15]. Overall, it appears that at any given set of conditions the prevailing balance between these two mechanisms is critical.

2. Methods

A detailed list of the equipment and supplies used in this work can be found in the data repository (see below).

2.1. Ethics statement

Animal care, breeding and experiments were carried out following the animal handling procedures conforming with the Guide for the Care and Use of Laboratory Animals published by the US National Institutes of Health and National Research Council of the National Academy of Sciences (NIH Publication No. 85–23) and with ethics approval by the State Veterinary Administration and according to Swiss Federal Animal protection law (permit BE 6/19).

2.2. Cell isolation

Ventricular myocytes were isolated from heterozygous mice carrying the mutation RyR2$^{R420Q+/−}$ or WT (RyR2$^{R420Q-/-}$) littermates as previously described [16]. In short, 4–8 months old male mice were euthanized by cervical dislocation and the hearts were excised, cannulated and retrogradely perfused on a custom made Langendorff system. Hearts were perfused at 37 °C for 15 min with modified Tyrode solution without added Ca^{2+} containing 160 U/ml collagenase type II (Worthington, New Jersey, USA) and 0.21 U/ml protease type XIV (Sigma, Buchs, Switzerland). After digestion was complete, ventricular myocytes were mechanically separated and filtered from undigested tissue with a 100 μm mesh filter (Corning™, North Carolina, USA). Cells were kept at room temperature while gently shaking in Tyrode modified solution with 250 μM added Ca^{2+} and used for experiments within 6 h after isolation.

2.3. Solutions

Solution constituents are expressed in mM unless stated otherwise.

2.3.1. Solutions for intact cell preparations

2.3.1.1. Tyrode modified solution. Basic composition: 140 NaCl, 5.4 KCl, 1.1 MgCl$_2$, 10 HEPES, 1 NaH$_2$PO$_4$, and 10 glucose (pH 7.4, adjusted with NaOH). EGTA, Ca^{2+} or other reagents were added as described within the text.

2.3.1.2. External solution. 140 NaCl, 5.4 KCl, 1.1 MgCl$_2$, 5 HEPES, 10 glucose and 1.8 CaCl$_2$ (pH 7.4, adjusted with NaOH).

2.3.2. Solutions for permeabilized cell preparations

2.3.2.1. Washing internal solution. 120 K-aspartate, 3 K$_2$ATP, 3 MgCl$_2$, 0.1 EGTA, 10 phosphocreatine, 10 HEPES and 5 U/ml creatine phosphokinase (pH 7.2, adjusted with KOH).

2.3.2.2. Permeabilizing solution. 100 K-Aspartate, 20 KCl, 3.7 MgCl$_2$, 1 EGTA, 10 HEPES, 0.005% Saponin (pH 7.2, adjusted with KOH).

2.3.2.3. Final internal solution. 120 K-aspartate, 3 K$_2$-ATP, 3 MgCl$_2$, 0.1 EGTA, 10 phosphocreatine, 10 HEPES, 5 U/ml creatine phosphokinase, 4% dextran 40K (pH 7.2, adjusted with KOH). Ca^{2+} concentration was adjusted to trigger waves or sparks as indicated using the Ca^{2+} calibration buffer kit (Life Technologies, Eugene, USA) with a fluorospectrometer (Nanodrop 3300, Thermo Fisher Scientific, USA) and the Ca^{2+} indicator Indo-1 (Biotium, Fremont, USA).

Please note that unlike some other reports [17], in our experimental conditions, even 20 min of permeabilization did not modify the S2808 phosphorylation level (see supplementary fig. S5 in [18]). The divergence between the studies is unknown but may lie in the permeabilization procedure itself. We also know that PKA signaling remains functional, since adding cAMP increases Ca^{2+} wave frequency after 5 min (see fig. S6 in [18]).

2.4. Fab preparation

Diffusion of the 2D12 PLB antibody (Thermo Fisher Scientific, USA) in permeabilized cells was facilitated by generation of Fab fragments as previously described [18,19]. 2D12 Fab fragments were produced using a commercial kit (Thermo Fisher Scientific, Rockford, USA). After the Fab fragment was generated and purified, traces of sodium azide or other contaminations derived from the kit were removed by dialysis using the DiaEasy Dialyzer MWCO 25 kD (BioVision, Milpitas, USA). Concentration of the Fab fragment was assessed by absorbance at 280 nm with a spectrophotometer (Q9000B UV–Vis Micro/Volumen Spectrophotometer, Quawell, China).

2.5. Confocal Ca^{2+} measurements

2.5.1. Ca^{2+} waves in intact cells

Cells were loaded with the Ca^{2+} indicator Fluo-3-AM (Biotium, Fremont, USA) at 5 μM for 30 min at room temperature and placed onto the microscope chamber. Ca^{2+} fluorescence signals were acquired with a

laser-scanning confocal microscope (FluoView1000, Olympus, Tokyo, Japan) equipped with a water immersion objective (UPlanS Apo 60 × 1.2 NA, Olympus, Tokyo, Japan). A 473 nm solid-state laser (Changchun New Industries Optoelectronics Tech, Changchun, China) was used to excite Fluo-3 and emitted fluorescence was measured at >500 nm. Cells were constantly bathed with the modified Tyrode solution and paced with an electrical field stimulator for 30 s at 1 Hz (0.5 ms, 20–40 V). Recordings in line-scan mode were taken before and after incubation with 0.1 μM isoproterenol (ISO) for 3 min. Wave latency, occurrence and frequency were quantified in each condition during the first 10 s after field stimulation. Kinetics features of the waves were also studied as detailed in the image analysis section. These and all other experiments were carried out at room temperature.

2.5.2. Ca²⁺ waves in permeabilized cells

Permeabilization of the cells was carried out as described previously [20,21]. Briefly, after cells were washed with Ca^{2+} − free Tyrode's solution supplemented with 100 μM of EGTA, myocytes were exposed to the *washing internal solution* for 30 s. Cells were then centrifuged at 0.4 $\times g$ for 1 min and the pellet was re-suspended for 30 s in the *permeabilizing solution*. Myocytes were centrifuged at 0.4 $\times g$, 1 min and the pellet was resuspended in the *final internal solution* containing 90–110 nM free Ca^{2+} and 12.5 μM Rhod-2 salt (Biotium, Fremont, USA). Permeabilized cells were seeded onto coverslips and placed on the confocal chamber for recordings. Rhod-2 was excited at 561 nm with a solid-state laser (Changchun New Industries Optoelectronics Tech, Changchun, China) and fluorescence was detected at >585 nm. The various pharmacological compounds were directly added to the experimental chamber.

2.5.3. Intra-SR Ca²⁺ measurements

Simultaneous cytosolic and SR Ca^{2+} changes were detected as previously described [20]. Cells were incubated with the low affinity Ca^{2+} indicator Fluo-5N-AM (Thermo Fisher Scientific, Hillsboro, USA) at 37 °C for up to 3 h to load the SR lumen. Following incubation, cells were permeabilized as described above. 12.5 μM of Rhod-2 salt was added to the final internal solution containing 100 nM Ca^{2+} supplemented with 2,3-Butanedione monoxime (BDM) (10 mM) (Sigma, Buchs, Switzerland) to reduce movement artefacts. Cells were seeded on coverslips coated with Cell-Tak (Corning™, C354240). Fluo-5N was excited at 473 nm and fluorescence was detected between 515 and 585 nm. The Rhod-2 signal of the cytosolic Ca^{2+} concentration was acquired as described above.

2.5.4. Spark recovery analysis

Intact cardiac myocytes loaded for 30 min at room temperature with 5 μM Fluo-3-AM and 5 μM EGTA-AM (AAT Bioquest, Sunnyvale, USA) were placed in the recording chamber in a modified Tyrode solution supplemented with 1 mM Ca^{2+}. After 30 min of waiting time for de-esterification, low dose of ryanodine (50 nM; Alomone Labs, Jerusalem, Israel) was used to evoke repetitive Ca^{2+} sparks [22]. A fresh aliquot of ryanodine was used for each experimental day. Ryanodine exposure for each myocyte was limited in time to avoid the appearance of long-lasting Ca^{2+} sparks. Before recording, cells in the isoproterenol (ISO) experimental group were exposed to 100 nM ISO for 3 min. Experimental solution containing 100 nM ISO and 50 nM ryanodine was subsequently applied to these cells. Ca^{2+} sparks were recorded using Fluo-3 excited at 488 nm with a solid-state laser (Coherent, Santa Clara, USA) and fluorescence was recorded above 500 nm. Repetitively firing clusters were identified and scanned with a confocal microscope (FluoView1200, Olympus, Tokyo, Japan) using a 60× water immersion objective (UPlanS Apo 1.2 NA) operated in line-scan mode.

2.6. Image analysis

Confocal line-scan images of Ca^{2+} waves were processed and analyzed using the software ImageJ. A custom macro was developed to align and de-skew the Ca^{2+} waves before analyzing these signals. Wave features such as amplitude ($\Delta F/F_0$) and τ (time constant of a single exponential decay fit) were quantified in de-skewed waves. For the intra SR Ca^{2+} recordings, photobleaching correction of the global signal was applied. The resulting measurements were expressed as $\Delta(F/F_{Caff})$, where F_{Caff} is the fluorescence recorded after depleting the SR with 10 mM caffeine [20]. The analysis of the line-scan recordings for sparks recovery was performed by a custom program written in Matlab (MathWorks). The same criteria for selection were applied as in [18]. Briefly, cells with Ca^{2+} spark frequencies higher than 15/100 μm/s, or cells with long-lasting sparks (> 200 ms), were excluded. Moreover, signals with 2 sub-populations of events (in terms of amplitudes of releases) were excluded since they might reflect the overlap of two clusters of RyR2. A bootstrapping approach was adopted to calculate 95% confidence intervals for the spark-to-spark delay medians [23].

2.7. Western blotting

Freshly isolated cardiomyocytes kept in control conditions or treated with ISO (1 μM) were incubated for 15 min while shaking gently. Cells were lysed with the NP-40 lysis buffer (Thermo Fisher Scientific, Rockford, USA) supplemented with anti-proteases (Complete Mini, Roche, Mannheim, Germany) and anti-phosphatases (PhosSTOP, Roche, Mannheim, Germany). Myocytes were centrifugated at 67 $\times g$ and the pellet was snap-frozen in liquid nitrogen and kept at −80 °C for later use. Following protein quantification using a commercial kit (Pierce BCA protein assay kit, Thermo Fisher Scientific, Rockford, USA), proteins were heated at 50 °C for 10 min and separated in reducing conditions by a 4–20% SDS-PAGE gradient stain-free gel (Bio-Rad, Hercules, USA) for 60 min at 200 V (Mini-PROTEAN® Tetra Vertical Electrophoresis Cell, Bio-Rad, China). 30–40 μg of proteins were loaded per lane. Separated proteins were transferred to a 0.45-μm pore size PVDF membrane (Millipore, Darmstadt, Germany) using the Trans-Blot® Turbo™ Transfer System (Bio-Rad, Singapore). The membranes were subsequently blocked for 1 h at room temperature in PBS-3% with bovine serum albumin (BSA). Membranes were incubated overnight with primary antibodies: anti-phospho-RyR2-S2808 (dilution 1:2000, Badrilla, Leeds, UK), anti-phospho-RyR2-S2814 (dilution 1:500, Badrilla, Leeds, UK) and anti-phospho-RyR2-S2030 (dilution 1:1000, custom made, Dr. H.H. Valdivia, Wisconsin, USA) or anti-RyR2 (dilution 1:1000, Abcam, Cambridge, UK). After several washings, the membranes were incubated with secondary anti-mouse or anti-rabbit antibodies conjugated to horseradish peroxidase (dilution 1:10,000, Jackson ImmunoResearch, Cambridgeshire, UK). Immunobinding reaction was detected using the Westar ECL Substrate (Westar Sun and Westar Supernova, Cyanagen, Bologna, Italy) and chemiluminescence signal was acquired with a ChemiDoc MP Imaging System (Bio-Rad). Protein density was quantified with the Image Lab Software (Life Science Research, Bio-Rad). A common reference sample was used among gels for internal normalization and allow pooling of samples ran at different days. Resulting signals were normalized to the total protein of each sample and phospho-RyR2 signals were subsequently normalized to the RyR2 level at control conditions for WT and CPVT samples respectively.

2.8. Statistics

Data are shown as mean ± SD or as otherwise stated. Numeric values are displayed as superplots [24] using violin plots, where the distribution of the entire dataset including animals and cells are shown. Violin plots represent estimated distributions of pooled cell data, where the number of animals (*N*) are represented by bigger circles and the number of cells (*n*) are small circles. In the wave kinetics parameters, multiple waves coming from a cell were averaged at the different treatments respectively. Non-paired Wilcoxon rank sum test was used for hypothesis testing on groups and hierarchical test analysis was used to confirm

and validate hypothesis testing on clusters at the animal level of waves parameters as described by others [25]. Matlab or R software was used to perform statistical analysis. Significance code presented in the figures: ns = no significance, $*p < 0.5$, $**p < 0.01$, $***p < 0.001$, $****p < 0.0001$.

3. Results

3.1. Arrhythmogenic Ca^{2+} signals are extensive in intact CPVT cardiomyocytes during β-adrenergic receptor stimulation

After an initial control experiment, intact cardiomyocytes were exposed to the β-adrenergic receptor agonist isoproterenol (ISO) and spontaneous Ca^{2+} waves were quantified from confocal line-scan recordings following a train of electrical pulses (30 s at 1 Hz, Fig. 1A). The cumulative occurrence of waves at various time points can be observed in Fig. 1B. Although the recording of Ca^{2+} events lasted much longer (40 s) and the presence of waves persisted in some cases, we considered only the first 10 s for quantitative analysis (blue vertical line in Fig. 1B) since later events were presumably not directly resulting from the

preceding field stimulation. At 10 s after the last pulse in control conditions, waves were only present in CPVT cardiomyocytes (and only in 10%), while in cells from WT littermates they were not observed at all (Fig. 1C). ISO treatment incremented the occurrence of waves to 90% in CPVT cells while in WT myocytes only 58% showed waves. These observations are consistent with the presence of the pro-arrhythmogenic phenotype we observed previously in these cells in different experimental conditions [13].

An additional indicator for the arrhythmogenicity of Ca^{2+} signals is the latency from the last electrically evoked Ca^{2+} transient to the first spontaneous Ca^{2+} wave (dashed horizontal black lines in Fig. 1A). Quantification of the latency revealed a significant shortening of this interval in CPVT cardiomyocytes when exposed to ISO as compared to WT (almost 2-fold shorter latency in the CPVT cells as compared to WT, Fig. 1D, $p = 0.02$). Not surprising, this result coincided with an elevated frequency of spontaneous Ca^{2+} waves in the CPVT cells that can be observed in Fig. 1E.
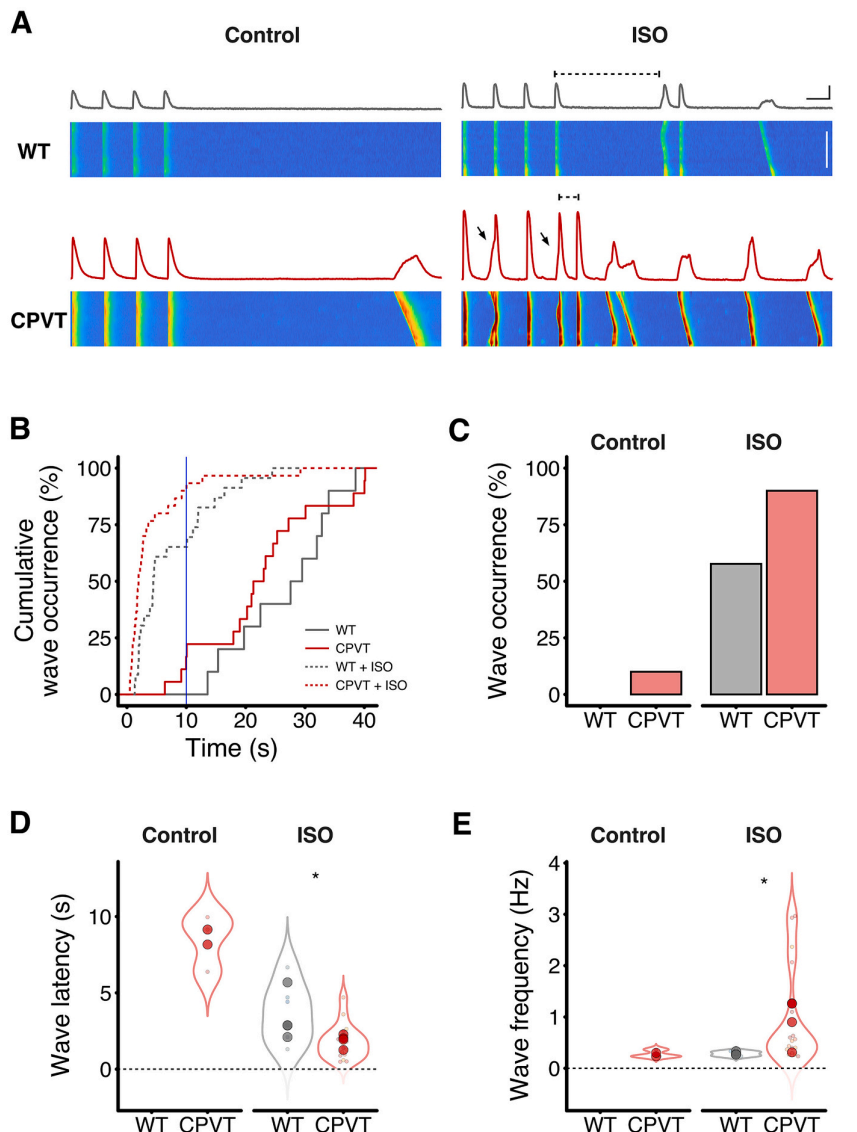

Fig. 1. Arrhythmogenic Ca^{2+} waves are more frequent in CPVT cardiomyocytes. (A) Representative line-scan images and plot profiles from WT and CPVT cells treated with ISO and control conditions. The transients seen at the beginning of the image are evoked from the last four electrical field stimulated pulses. The horizontal dashed line highlights the wave latency differences between WT and CPVT cells under ISO treatment. Note the arrow indicating initiation of premature waves in the line-scan of CPVT cell treated with ISO within two consecutive electrical pulses. Scale bar for line-scan images (white): 40 μm; horizontal and vertical scale bars for traces (black): 1 s and 1.5 $\Delta F/F_0$ respectively. (B) Cumulative occurrence of waves for the full recording. The blue vertical line indicates the time for which relative occurrence (C), latency (D) and frequency (E) were determined. Data points in (D) and (E) are from cells which showed waves. N and n of waves analyzed: WT $N = 4$, $n = 26$ and CPVT $N = 5$, $n = 30$. On wave occurrence, contingency table of total cells was assessed using pairwise Fisher exact test and the Benjamini & Hochberg (BH) p adjusted method for multiple comparisons. On wave latency and frequency, statistical differences were assessed using the Wilcoxon rank sum test only in cells under presence of ISO, since at 10 s recording duration in control conditions no waves were present in WT. (For interpretation of the references to colour in this figure legend, the reader is referred to the web version of this article.)

3.2. Ca²⁺ wave kinetics show larger Ca²⁺ release in CPVT cardiomyocytes

The above results indicate that cardiomyocytes carrying the RyR2$^{R420Q+/-}$ mutation had a higher propensity to generate potentially arrhythmogenic Ca²⁺ waves, particularly during ß-adrenergic receptor stimulation. To gain deeper insight in the nature of this arrhythmogenic signals we analyzed the kinetic properties of de-skewed Ca²⁺ waves in more detail (see methods). Representative line-scan images showing Ca²⁺ waves in control condition and after ISO treatment are shown in Fig. 2A. Detailed statistics on the kinetics of the Ca²⁺ waves are presented in the supplementary Table 1. Fig. 2B depicts profiles of averaged de-skewed traces of Ca²⁺ waves. The quantitative analysis revealed a comparable decay time constant (τ) in control conditions and its expected shortening during ISO stimulation in both cell types (Fig. 2D). Similar observations were made regarding the wave velocity (Fig. 2E). The amplitude of waves in CPVT cardiomyocytes were larger in control conditions and no further increment was observed when ISO was applied (Fig. 2C and supplementary Table 1).

3.3. Specific SERCA stimulation increases arrhythmogenic Ca²⁺ events in permeabilized cardiomyocytes of CPVT mice

β-adrenergic receptor stimulation unfolds a signaling cascade that causes the production of cAMP and activation of protein kinase A (PKA), which ultimately phosphorylates a number of substrates including RyR2 and phospholamban. The latter, upon phosphorylation, is uncoupled from SERCA thus removing its inhibition and enhancing the Ca²⁺ uptake to the SR. Overload of Ca²⁺ in the SR after SERCA stimulation or changes of the Ca²⁺ wave generation threshold resulting from RyR2 phosphorylation have both been shown to be important factors for Ca²⁺ wave arrhythmogenesis [12]. Thus, both RyR2 phosphorylation and SERCA stimulation could be molecular mechanisms responsible for or contribute to the generation of arrhythmogenic Ca²⁺ waves in CPVT cardiomyocytes during β-adrenergic receptor stimulation.

To get further insight into the mechanisms contributing to wave arrhythmogenicity in CPVT cardiomyocytes upon β-adrenergic receptor stimulation, we decided to specifically stimulate the SERCA only (i.e. without changing the extent of RyR2 phosphorylation). Specific stimulation of the SERCA can be achieved with the antigen-binding fragment (Fab) of the 2D12 phospholamban antibody [18]. Application of Fab fragments promotes the disinhibition of SERCA, therefore mimicking the effect of β-adrenergic stimulation specifically on the SERCA activity without affecting other phosphorylation targets. Permeabilized cardiomyocytes were treated with the Fab fragment or, for comparison, with cAMP (to mimic β-adrenergic receptor stimulation) and the frequency of Ca²⁺ waves was quantified. 5–7 min were allowed for the drug to obtain a stable response.

Fig. 3A shows representative line-scan images and profiles of Ca²⁺ signals from permeabilized cells. Application of Fab 30 μg/ml elevated the wave frequency 5.7-fold ($\pm$1.6) in CPVT cells while in the myocytes from WT littermates the increment was 4.0 $\pm$ 1.4 ($p = 0.024$). Of note, cAMP administration raised the wave frequency to a much lesser extent than the Fab fragment (Fig. 3B) and was comparable between the two cell groups (normalized frequency WT-cAMP = 2.4 $\pm$ 0.6, CPVT-cAMP = 2.1 $\pm$ 0.6, $p = 0.49$). Fig. 3C and D summarize statistics of the Fab and
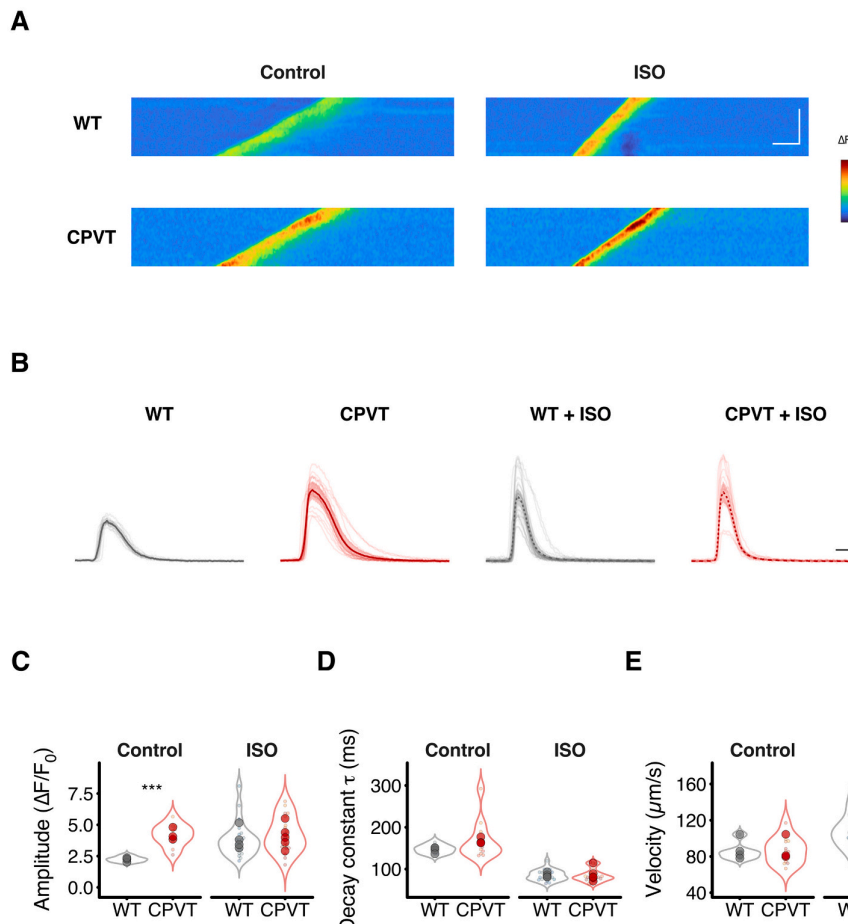

Fig. 2. Analysis of spontaneous Ca²⁺ wave kinetics in CPVT and WT cardiomyocytes. (A) Representative line-scan images showing waves in detail of CPVT and WT cardiomyocytes in control and in ISO conditions. Horizontal and vertical scale bar for line-scan images (white) = 50 ms, 40 μm. (B) Average of individual traces $\pm$95% confidence intervals of Ca²⁺ waves. Horizontal and vertical scale bar for traces (black): 200 ms, 1 ΔF/F₀. Note that the wave amplitude in the CPVT cells was already larger in control conditions. De-skewed waves were analyzed (see methods) and the summary statistics of wave amplitude, decay time constant and velocity of de-skewed waves are shown in (C), (D) and (E), respectively. See supplementary Table 1 for summary of results.

A

B

C

D
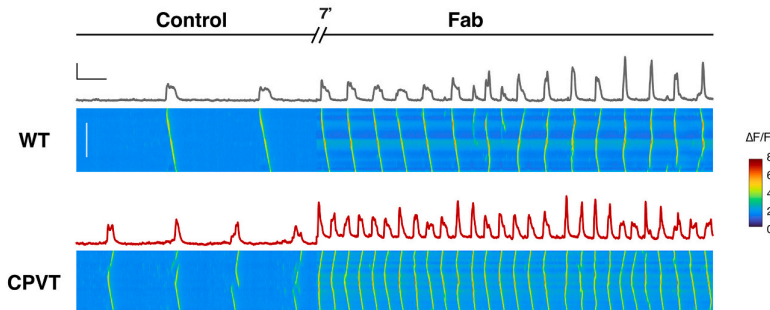
Fig. 3. Specific SERCA stimulation increases frequency of Ca^{2+} waves in permeabilized cardiomyocytes. Line-scan and fluorescence profiles traces of Ca^{2+} signals from permeabilized cells treated with Fab 30 µg/ml or cAMP 20 µM are shown in (A) and (B) respectively. Following the drug application, recording was resumed after 7 min incubation time as indicated. Scale bar for line-scan images (white): 50 µm. Horizontal and vertical scale bars for traces (black): 2.5 s, 0.5 $\Delta F/F_0$. Normalized frequency to the time before the drug application (control) and after incubation with Fab or cAMP is shown in (C) and (D) respectively. N and n of waves analyzed for panel (C): WT, $N = 5$, $n = 11$; CPVT, $N = 4$, $n = 10$. And for panel (D): WT, $N = 5$, $n = 15$; CPVT, $N = 5$, $n = 14$. Statistical differences were assessed using the Wilcoxon rank sum test.
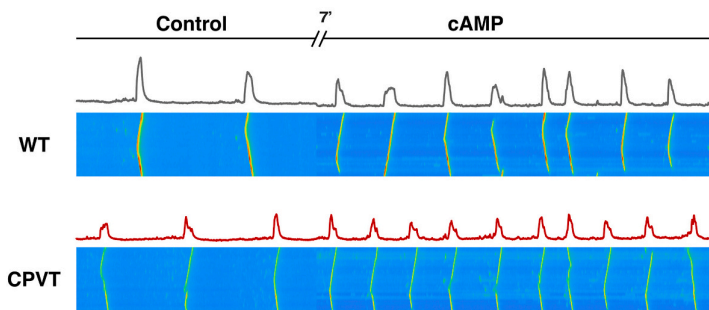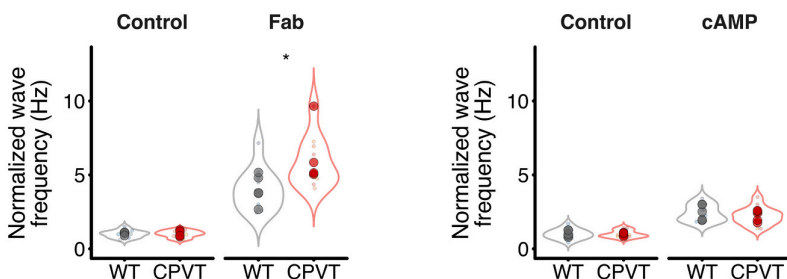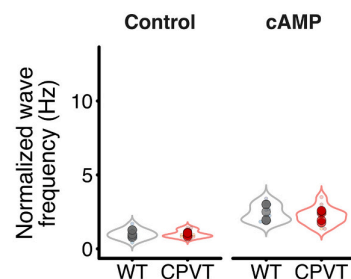
cAMP effect on the wave frequency. These results could be explained by a more pronounced sensitization of mutated RyR2s after PKA dependent phosphorylation (see below). This could lead to a larger SR Ca^{2+} leak in CPVT cells during cAMP exposure, essentially reducing the SR load somewhat. As a consequence, this leak could limit the increase in wave frequency, while during specific SERCA stimulation with Fab fragments this leak would not be present.

3.4. Specific SERCA stimulation reveals changes in Ca^{2+} wave kinetics of permeabilized CPVT cardiomyocytes

We found that direct SERCA stimulation with the Fab fragment elevated the wave frequency in CPVT more than in WT cardiomyocytes (Fig. 3). Also, Fab surprisingly caused a considerably larger increment in wave frequency than exposure to cAMP (Fig. 3C and D). Could this difference result from a stronger SERCA stimulation by Fab than by cAMP? Or could it be explained by an SR Ca^{2+} leak and unloading via phosphorylated RyR2s, that was only present in cAMP but not with Fab

stimulation of the SERCA? From previous work we know that under these conditions both the Fab fragment and cAMP lead to near maximal stimulation of the SERCA (see fig. S6 in [18]). To gain additional information we decided to examine wave kinetics when initiating downstream activation of the β-adrenergic signaling pathway with cAMP and the specific SERCA agonist Fab (Fig. 4). Representative line-scan images showing Ca^{2+} waves and averaged profile traces derived from deskewed waves are shown. Detailed analysis of the wave kinetics in deskewed waves from permeabilized cells confirmed comparable stimulation of SERCA activity in cAMP and Fab, as measured by the decay time constant of the waves (τ) (see supplementary Table 2 and Fig. 4C, F middle panel). There is a potential problem when comparing wave decay kinetics to compare SERCA activities. In cAMP the wave decay kinetics could be slightly slowed by the SR Ca^{2+} leak. Our observation of identical decay kinetics would then mean that SERCA in cAMP is faster than in the presence of Fab. This would lead to a higher wave frequency in cAMP than in Fab. However, this is the opposite of what we observed here. Therefore, this problem can be ruled out as a reason for higher
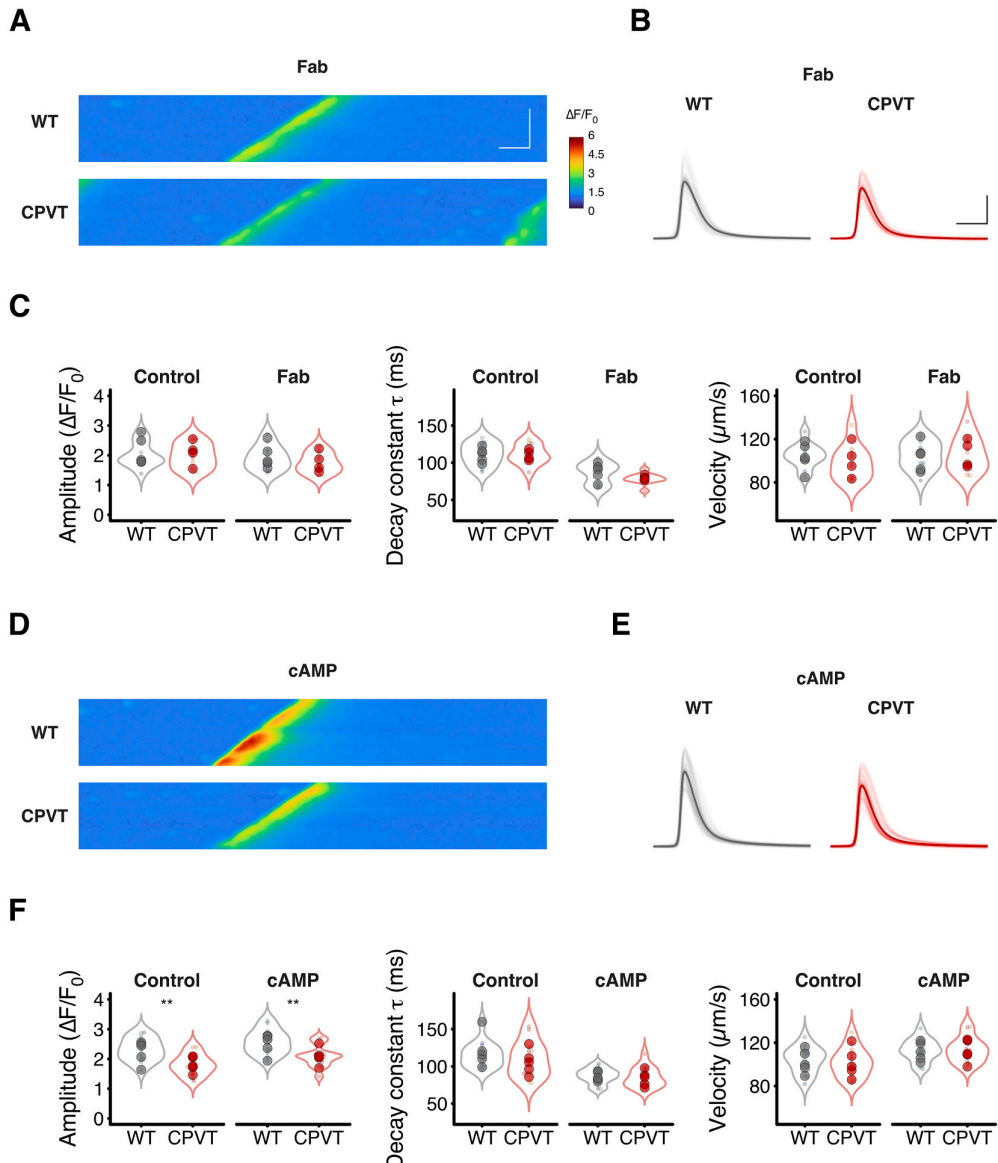
Fig. 4. Both cAMP and Fab enhance SERCA activity in permeabilized CPVT cardiomyocytes. Representative line-scan images of Ca^{2+} waves in permeabilized WT and CPVT cardiomyocytes under Fab (A) or cAMP (D) treatments. Horizontal and vertical scale bar for line-scan images (white): 100 ms, 25 μm. (B) and (E) show averaged plot profiles of de-skewed traces from cells treated with Fab and cAMP respectively. Horizontal and vertical scale bar for traces (black): 200 ms, 1 $\Delta F/F_0$. (C) and (F) are the resulting summary statistics of the amplitude and decay time constant (τ) of de-skewed waves and wave velocity of cells treated with Fab and cAMP respectively. See supplementary Table 2 for additional details.

wave frequencies in Fab. Thus, taken together different SERCA activities could not explain the disparities in wave frequencies in cAMP and Fab noted above. In addition, these experiments revealed an increment in the amplitude of the waves in the WT cells by 20 μM cAMP (Fig. 4F left panel and supplementary Table 2). The wave velocity in the CPVT cells and WT was increased to a fairly comparable extent under cAMP (Fig. 4F right panel). On the other hand, Fab application seemed not to affect the amplitude nor the velocities of Ca^{2+} waves in the WT or CPVT mutant cells (Fig. 4C right and left panels). Taken together, these findings indicate that SERCA stimulation by cAMP and Fab was comparable and SERCA activity can therefore not be responsible for the substantial differences in wave frequencies shown in Fig. 3.

3.5. Sensitivity of CICR is augmented in CPVT cardiomyocytes in basal conditions and it is exacerbated under β-adrenergic receptor stimulation

Several of our findings above could be explained by a higher Ca^{2+} sensitivity of CICR in the presence of the mutated RyR2s. This might be exacerbated during application of cAMP (but not so much during exposure to Fab). Indeed, a variety of CPVT mutations in the *RyR2* gene have been described, in which many confer gain of function of the Ca^{2+} release channel [6,26,27]. In our CPVT animal model, we examined changes of CICR Ca^{2+} sensitivity in-situ by analyzing the Ca^{2+} spark recovery kinetics. Briefly, one RyR2 channel within a cluster is modified by a very low concentration of ryanodine. This channel is thought to drive a cluster which fires repetitive Ca^{2+} sparks that are further studied in detail to evaluate the Ca^{2+} sensitivity of CICR and the RyR2s [28,29].

The median of the spark-to-spark probability distribution is a parameter believed to reflect the Ca^{2+} sensitivity of the RyR2s, or, in a wider sense, the Ca^{2+} sensitivity of CICR [28]. The spark amplitude recovery kinetics reflects the local Ca^{2+} store refilling, and is largely governed by intra-SR Ca^{2+} diffusion, with a small contribution by SERCA activity [30]. Representative line-scan images showing repetitive spark events can be observed in Fig. 5A. The spark-to-spark delay was analyzed to estimate the sensitivity of CICR in control conditions and under β-AR stimulation (Fig. 5B–C). In control the medians of the probability distribution of the spark-to-spark delays in mutant cardiomyocytes were significantly shorter than WT, indicating an enhanced basal in-situ CICR sensitivity in the CPVT cells. Application of isoproterenol shifted the median of the
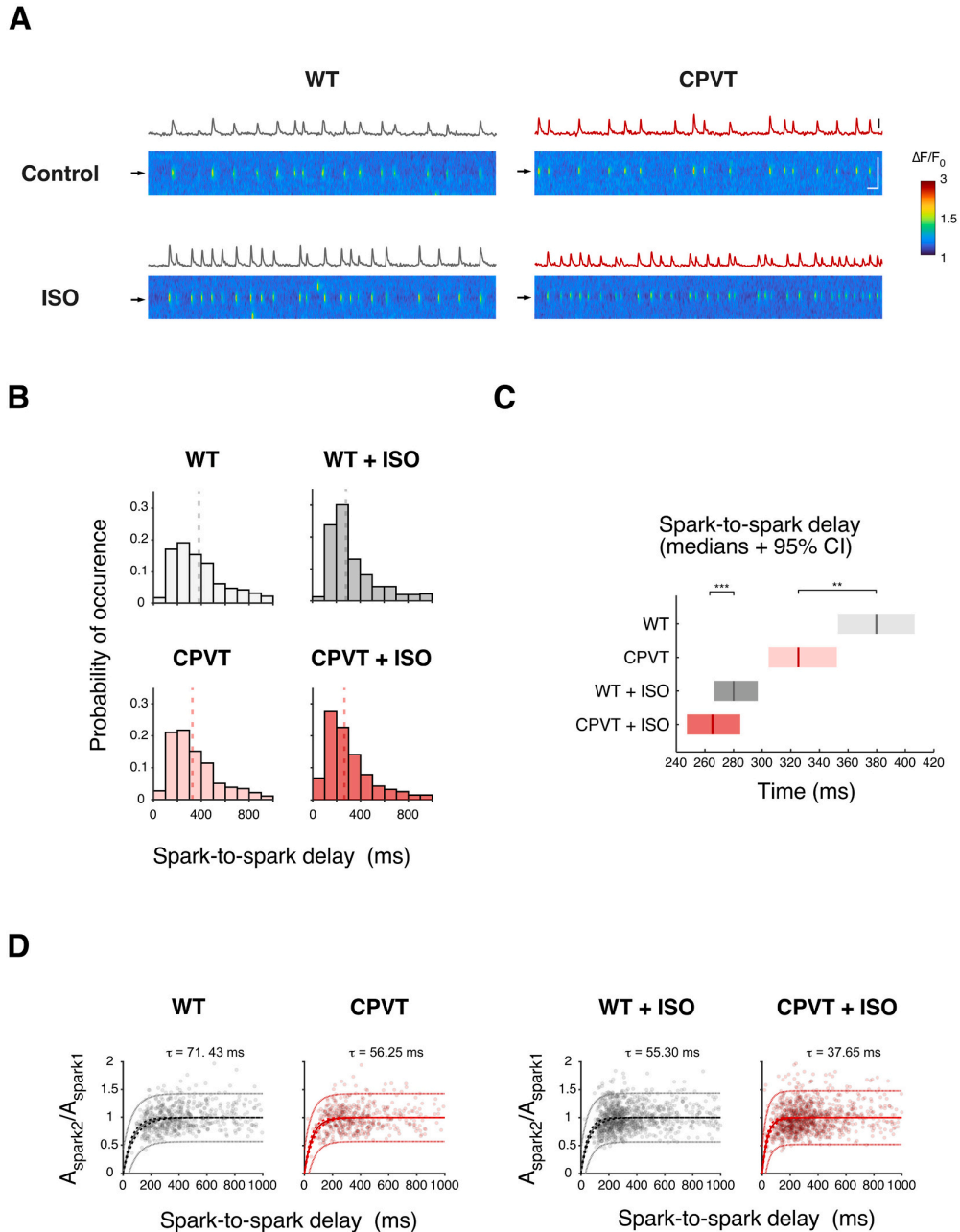

Fig. 5. CICR in mutant CPVT cardiomyocytes showed enhanced Ca^{2+} sensitivity during spark recovery in the presence of 50 nM ryanodine. (A) Representative line-scan images and profiles showing repetitive sparks. The arrow indicates the region taken to generate plot profiles. Horizontal and vertical scale bar respectively for images: 200 ms, 10 µm. Vertical scale bar for traces 0.5 ΔF/F_0. (B) Histograms of delays of Ca^{2+} sparks in control conditions and in presence of 100 nM ISO in WT and CPVT cardiomyocytes. The vertical dashed lines in the histograms represent the medians of the spark-to-spark delay distributions. (C) Summary of all medians of spark-to-spar delays with their 95% confidence interval. The star shows statistical difference in the spark-to-spark delay of the indicated groups assessed with Kruskal-Wallis with Scheffé's *p* adjusted method. (D) Spark amplitude restitution of WT and CPVT cells in control and under 100 nM ISO stimulation. Every graph represents the normalized amplitude of the second spark versus the delay between pairs. Data were fitted to a single exponential function (continuous line) and calculated 95% confidential interval and prediction interval are indicated with long and short dashed lines respectively. See supplementary Table 3 for summary of results.

distribution in CPVT cells to a larger extent (left shift) as compared to WT, suggesting a marked gain in Ca^{2+} sensitivity. Fig. 5B shows the distributions of spark delays obtained in control conditions and under isoproterenol treatment for CPVT and WT cells and the summary of medians with confidence intervals are displayed in Fig. 5C.

We also analyzed the amplitude restitution of the sparks (Fig. 5D), a parameter that describes the relationship between the relative spark amplitude and the spark-to-spark delay and provides information on the recovery of local SR Ca^{2+} content (see details in methods). This parameter is known to be accelerated following SERCA stimulation during activation of the β-adrenergic pathway [23] although most of the local SR Ca^{2+} refilling after a spark occurs by intra-SR Ca^{2+} diffusion. We found that in our CPVT mutant cells, the τ (recovery time constant) of the spark amplitude was significantly shorter at basal conditions. This could result from the SR remodeling known to occur in these myocytes, with overall reduced CSQ expression [13]. Application of isoproterenol accelerated the rate of spark amplitude restitution in CPVT cells by approximately 20 ms more than in WT cells, indicating faster local SR Ca^{2+} refilling under β-adrenergic stimulation. Detailed statistics for the spark-to-spark recovery analysis and the amplitude restitution of the sparks is shown in supplementary Table 3. In summary, these findings confirm that in situ CICR and the RyR2s of CPVT myocytes are more sensitive and can be re-activated more quickly after β-AR stimulation.

3.6. SERCA stimulation by cAMP and Fab differentially affect the SR Ca^{2+} wave threshold

The difference in CICR sensitivities observed with our spark recovery analysis is known to result in a higher SR Ca^{2+} leak and reduced SR Ca^{2+} content in cells harboring the mutation [13]. In addition, exposure of the permeabilized myocytes to Fab or cAMP could affect SR Ca^{2+} quite differently. Both will stimulate the SERCA, but in cAMP the PKA activation may also lead to RyR2 phosphorylation, which in turn could add yet another SR Ca^{2+} leak, resulting in lower SR Ca^{2+} content. To explore the contribution of the SERCA and the Ca^{2+} leak to the intra SR Ca^{2+} concentration during β-adrenergic stimulation, we measured the intraluminal SR Ca^{2+} concentration of permeabilized cells during exposure to cAMP or Fab (see Fig. 6A). We quantified and normalized this value to the total Ca^{2+} concentration after the SR depletion with caffeine (see methods and [20,21]). Interestingly, the SR Ca^{2+} concentration was significantly lower in cAMP treated cells than in the presence of Fab (Fig. 6B), both in WT and CPVT myocytes. This observation is consistent with the notion that in cAMP an additional leak pathway is activated which reduces SR Ca^{2+} content. This does not occur in the presence of Fab. As noted before under control conditions [13], the CPVT mutant cardiomyocytes had an SR Ca^{2+} concentration that was slightly lower, both with cAMP treatment and in the presence of Fab (WT-cAMP = 0.28 ± 0.15, CPVT-cAMP = 0.24 ± 0.1, $p = 0.42$; WT-Fab = 0.43 ± 0.21, $p = 0.04$, CPVT-Fab = 0.36 ± 0.17, $p = 0.04$). This most likely reflects the higher CICR sensitivity of the cells with the mutated RyR2. See Fig. 7 for WB experiments confirming the PKA-dependent phosphorylation of the
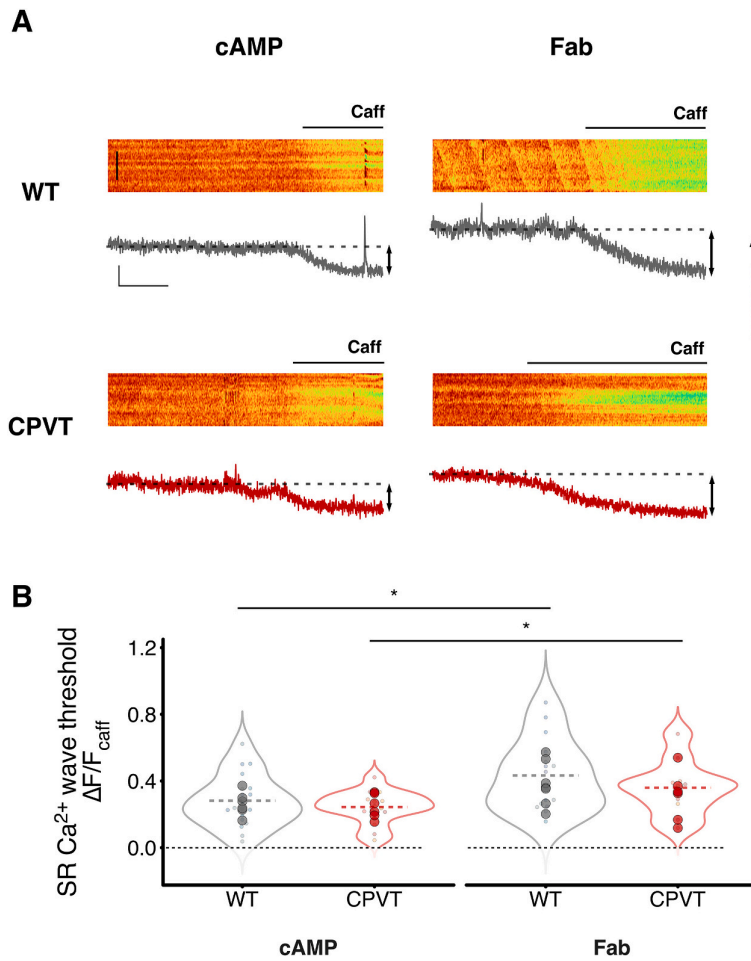

Fig. 6. Luminal SR Ca^{2+} content in CPVT mutant cells is higher under specific SERCA stimulation than in the presence of cAMP. (A) Representative traces of SR Ca^{2+} measurements in permeabilized cardiomyocytes stimulated with cAMP or Fab. Plot profiles of the images for the SR Ca^{2+} are displayed below each line-scan respectively. Note the relative level of the SR Ca^{2+} indicated by the dashed line and compared to total Ca^{2+} level after depletion of the SR with caffeine (Caff). Scale bar for line-scan images: 50 μm; horizontal and vertical scale bars for traces: 1.5 s and 0.1 $\Delta F/F_0$ respectively. (B) Summary statistics of the SR Ca^{2+} level measurements at the threshold of waves. SR Ca^{2+} was normalized to the maximum SR Ca^{2+} content after Caff application ($\Delta F/F_{caff}$). Dashed lines represent the median. N and n of cells analyzed for panel (B): WT-cAMP, $N = 6$, $n = 19$; WT-Fab, $N = 7$, $n = 16$; CPVT-cAMP, $N = 6$, $n = 15$; CPVT -Fab, $N = 6$, $n = 10$. Statistical differences assessed with two-way Anova and post hoc contrast determined with Tukey test with the BH p adjusted method. Scale bar in image = 50 μm.

A

P2030

P2808

P2814

B


C

RyR

D
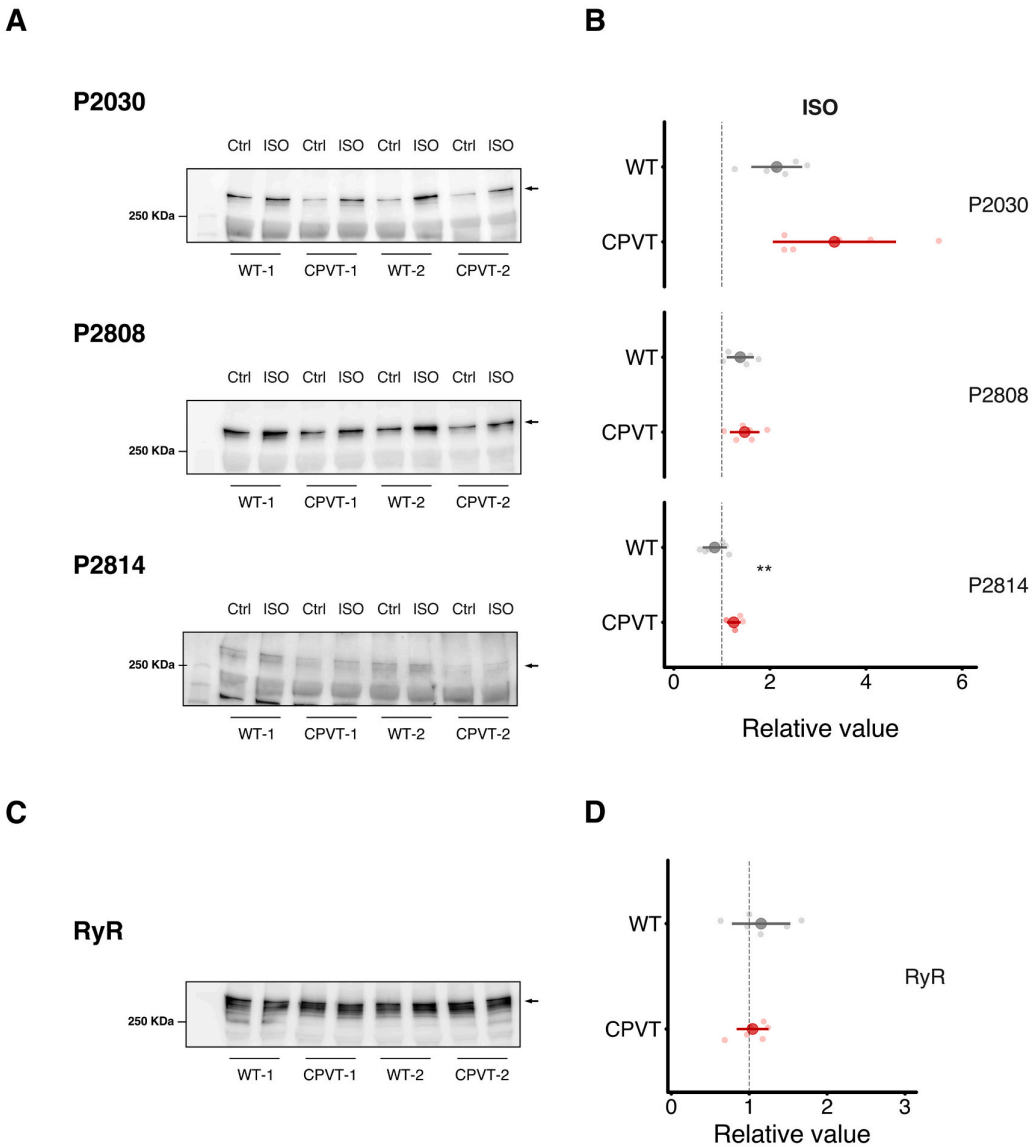
Fig. 7. Phosphorylation of RyR2 at serin 2030 is slightly augmented in myocytes from CPVT mice under ß-adrenergic stimulation. (A) Representative images of blots showing the immunostaining of RyR2 phosphorylation at serine 2030 (top), serine 2808 (middle) and serine 2814 (bottom) in WT and CPVT cardiomyocytes in control conditions (Ctrl) and stimulated with isoproterenol (ISO). The arrow indicates the band position of RyR2 in the blots. (B) Quantification of RyR2 phosphorylation increments under ISO stimulation relative to control conditions. The dashed lines are placed at the control position for the sake of comparison. Values as mean ± SD: WT-ISO = 2.15 ± 0.53, CPVT-ISO = 3.36 ± 1.28, $p = 0.09$ for the phospho-RyR2-S2030; WT-ISO = 1.39 ± 0.28, CPVT-ISO = 1.49 ± 0.31, $p = 0.60$ for the phospho-RyR2-S2808 and WT-ISO = 0.86 ± 0.53, CPVT-ISO = 1.26 ± 1.28, $p = 0.02$ for the phospho-RyR2-S2814. (C) Representative blot of total RyR2 immunostaining of different WT and CPVT cardiomyocytes preparations. (D) The total RyR2 quantification obtained from WT and CPVT cardiomyocytes. $N = 6$, $p = 0.55$. Significance assessed with *t*-test and *p* value adjusted with the BH method for multiples comparisons.

RyR2s under these conditions.

3.7. Phosphorylation of RYR2 shows signs of augmentation in the CPVT cells during β-adrenergic stimulation

To obtain a better understanding of the potential pathophysiological signaling pathways underlying stress-induced arrhythmias precipitated by the RyR$^{\text{R420Q}+/-}$ mutation, we investigated the phosphorylation of the RyR2 at the sites directly affected by the canonical pathway activated by the ß-adrenergic receptor stimulation. This well-known pathway involves ultimately the phosphorylation of RyR2 at the residues S2808 and S2030 by PKA [31–34]. We performed immunoblotting

experiments using isolated cardiomyocytes stimulated with isoproterenol and normalized the phosphorylation to untreated cells. Fig. 7A–B show representative blots of phospho-site specific antibody stainings and the resulting quantification, respectively. Both S2808 and S2030 showed a larger extent of phosphorylation in ISO. The dynamics in the S2808 phosphorylation is presumably less pronounced than that of the S2030 site due to its already high degree of phosphorylation under control conditions [18]. In the CPVT cardiomyocytes we observed a trend to a more pronounced phosphorylation compared to WT during exposure to ISO of S2030 ($p = 0.13$), while serine 2808 was increased to similar extents in both cell types (details in the figure legend). In addition, we examined the phosphorylation level at serine S2814, a known

target of CaMKII, which is Ca^{2+} dependent and can become activated indirectly during β-adrenergic stimulation. Although observing a consistent phosphorylation increment at the S2808 and S2030 phosphosites during ISO stimulation, the S2814 site did not become elevated in our conditions in the WT animals ($p = 0.237$, WT-ISO vs control) However, the CPVT cardiomyocytes were significantly more phosphorylated at S2814 in ISO ($p = 0.01$, WT-ISO vs CPVT-ISO).

To exclude the possibility that the changes observed in the RyR2 phosphorylation are due to different RyR2 expression, we checked the intrinsic levels of the total RyR2 protein of our CPVT mutant model. Representative RyR2 immunoblots of cardiomyocyte preparations are shown in Fig. 7C. Fig. 7D summarizes the quantification of total RyR2 in both animals revealing no significance differences, as has been noted before [13].

Taken together, our observations suggest a subtle increment of the phosphorylation levels of the S2030 residue in the CPVT myocytes under stress induced with isoproterenol, which are no due to changes of the total RyR2 expression.

4. Discussion

At present, more than 200 RyR2 mutations are known to cause life threatening arrhythmias in the affected patients [35,36]. However, the precise cellular and molecular mechanism(s) triggering the arrhythmia during emotional stress or physical exercise are not known. In fact, it may be not the same for each of the mutations. This was recently shown for a RyR2 loss-of-function mutation [7]. It is generally assumed and supported by experimental work on the cellular level that with gain-of-function mutations abnormal SR Ca^{2+} release events during diastole, such as Ca^{2+} waves, become more frequent. Ca^{2+} waves trigger DADs which can culminate in action potentials, causing extra beats and arrhythmias, provided a substantial number of cardiomyocytes generates them simultaneously. Obvious candidate mechanism responsible for abnormal diastolic Ca^{2+} release precipitated by stress could be RyR2 phosphorylation or the stimulation of SERCA leading to elevated SR Ca^{2+} loading. Both of these Ca^{2+} signaling pathways are boosted during ß-AR stimulation.

The gain-of-function mutation R420Q of the RyR2 channel has been identified and described in a family presenting with CPVT in some of its members [37]. Later, a genetically engineered mouse model based on this mutation was created, displaying arrhythmic features analogous to those of the human patients during stress [13,14].

In the present study we carried out experiments with cardiomyocytes isolated from the RyR2$^{R420Q+/-}$ mice and their WT littermates to define the specific roles for RyR2 phosphorylation and/or SERCA stimulation as mechanisms contributing to the arrhythmogenic Ca^{2+} signaling events.

During β-AR stimulation with ISO (to mimic stress), almost all RyR2$^{R420Q+/-}$ cells showed Ca^{2+} waves after a conditioning pre-pulse protocol. In fact, even before adding ISO, waves were observed in cells with mutated RyR2s, while none were present in WT myocytes. This was paralleled by higher wave frequencies and a shorter delay to the first wave after field stimulation in RyR2$^{R420Q+/-}$ cells. When the SERCA was selectively stimulated in permeabilized cells with a Fab fragment against PLB (e.g. no RyR2 phosphorylation occurred), wave frequency was strongly elevated in both, WT and RyR2$^{R420Q+/-}$ cell types, but more in cells harboring the mutation. Very much to our surprise, in the presence of cAMP, when SERCA stimulation as well as PKA-dependent RyR2 phosphorylation occurred simultaneously, wave frequencies increased much less than during selective SERCA stimulation.

4.1. Role of RyR2 in precipitating pro-arrhythmogenic events

Several findings of the present and previous [13,37,38] studies suggest an overall gain of CICR function in the cardiomyocytes harboring the RyR2$^{R420Q+/-}$ mutation. Even in the absence of ß-AR

stimulation, the mutant cells exhibited diastolic Ca^{2+} waves and produced a larger Ca^{2+} release when compared to cells from their WT-littermates (Fig. 2B–C). The differences in wave frequency and latency to first wave after a termination of a train of stimulations were even more pronounced during β-AR stimulation (Fig. 1).

Furthermore, our experiments assessing the time-course of recovery of RyR2 activity showed a left shift in spark-to-spark delay experiments, even in control conditions and much more so during ß-AR stimulation (Fig. 5), again indicating that CICR is more sensitive in the presence of the RyR2$^{R420Q+/-}$ mutation.

As described in other gain-of-function RyR2 mutations [6,27,39], leaky or sensitized mutant channels can contribute to the diastolic cytosolic Ca^{2+} concentration. They may further recruit and activate neighboring RyR2s clusters in a positive feedback loop that can ultimately result in arrhythmogenic Ca^{2+} waves. Thus, the reduced delay and the increased occurrence and frequency of waves we observed during β-AR stimulation (Fig. 1C–E) are also in line with the findings of abnormal Ca^{2+} oscillations in HEK-293 cells transfected with the RyR2^{R420Q} mutation [37].

Activation of the β-AR pathway induces PKA dependent phosphorylation of the RyR2 channel at well characterized residues (serines 2808, 2030) [18,31,40,41]. The resulting enhancement on Ca^{2+} dynamics can subsequently lead to phosphorylation at serine S2814, mediated by CaMKII. The RyR2$^{R420Q+/-}$ cardiomyocytes present no evident changes in total RyR2 expression and in S2808, S2030 and S2014 phospho-sites in control conditions (Fig. 7 and supplementary material in [13]). During ß-AR stimulation the phosphorylation levels showed the expected rise at these two sites, but the extent at S2030 was slightly higher in CPVT myocytes. Furthermore, the S2814 phosphorylation was incremented, but only in the CPVT cells. The reasons for this result are unknown but in our experimental conditions CaMKII may not become fully activated. The potential functional significance of this observation is not known, but we speculate that it may be related to structural molecular changes of the RyR2 recently reported for this mutation [13]. In any case, serine 2030, which exhibits the largest change in phosphorylation, has been recently reported to be crucially important for the RyR2 modulation during a ß-adrenergic response [18].

4.2. Role of SERCA stimulation in precipitating Ca^{2+} waves

Other factors may also contribute to the arrhythmogenic phenotype observed in CPVT cells, such as an enhanced availability of stored Ca^{2+} due to an incremented SR Ca^{2+} content. This is underscored by our observations after specific SERCA stimulation with the Fab fragment of a PLB antibody. Please note that the expression of SERCA and PLB is not altered in the CPVT animals [13]. In these experiments, the SERCA was stimulated to the similar extent as during addition of cAMP (Fig. 4E and F). The latter leads to SERCA stimulation after phosphorylation of PLB. Surprisingly, in both cell types the selective SERCA stimulation with the Fab fragment resulted in a much higher Ca^{2+} wave frequency than when the same SERCA stimulation was induced by cAMP and thus paralleled by PKA-dependent RyR2 phosphorylation (compare Fig. 3C and D). In the CPVT cells the wave frequency during selective SERCA stimulation increased even more than in WT cells (Fig. 3C). This most likely is a direct consequence of a reduced luminal SR Ca^{2+} wave trigger threshold in the CPVT mutant cells, as observed in a previous study [13].

In fact, a number of earlier studies have suggested that changes in the SR luminal Ca^{2+} concentration and store overload modulate the RyR2 activity [42–44]. Such changes can result in Ca^{2+} releases during diastole [45]. Furthermore, several RyR2-associated CPVT mutations have been described to have altered luminal SR Ca^{2+} threshold sensitivity for wave generation, being a major factor for arrhythmogenicity [46]. Together, these observations suggest a dynamic mechanism of SR refilling for eliciting arrhythmogenic Ca^{2+} waves in the cardiomyocytes, whereby the leaky mutant RyR2 channels with the R420Q mutation might increase the probability of triggering arrhythmogenic Ca^{2+} waves

further.

4.3. Reciprocal interplay between SERCA activity and RyR2 phosphorylation

How can it be that activation of only one of two potentially arrhythmogenic mechanisms (i.e. SERCA and RyR2 phosphorylation) paradoxically result in a higher prevalence of arrhythmogenic events? Why are these two mechanisms not behaving in an additive way? To resolve this puzzling observation, we have to consider the fact that both of these potentially arrhythmogenic mechanisms also can have anti-arrhythmic consequences (for details see Fig. 8). While SERCA stimulation will increase the SR Ca^{2+} load thereby contributing to spontaneous Ca^{2+} release events, it will also lower the cytosolic Ca^{2+} concentration, which will tend to reduce or interrupt the propagation of diastolic Ca^{2+} waves. Interestingly, this protective, yet paradoxical effect of high SERCA activity has been observed in other studies using a different RyR2-mutant CPVT mouse model which also lacks PLB, the regulatory protein of SERCA [47,48]. Thus, SERCA stimulation favors the generation of Ca^{2+} waves by loading the SR with Ca^{2+}, but by reducing the cytosolic Ca^{2+} concentration increases the threshold for

spontaneous Ca^{2+} waves and can interrupt their propagation [15]. Other cases for the importance of the interplay between SR loading, SERCA activity and arrhythmogenic events have been described in the literature. For example, a CPVT mouse model lacking calsequestrin expression (CSQ KO) has been cross-bred with a mouse overexpressing SERCA1 [49]. In the crossbred animals, the predominant consequence of high SERCA activity would be expected to result in SR Ca^{2+} overload, since the SR Ca^{2+} buffer capacity is dramatically reduced in these myocytes. Indeed, cardiomyocytes isolated from these mice exhibited very high wave frequencies.

In the case of the RyR2s, an enhanced Ca^{2+} leak after their phosphorylation not only leads to more spontaneous cytosolic Ca^{2+} signaling events potentially provoking Ca^{2+} waves, but also results in a retardation of SR Ca^{2+} refilling and a reduction of the SR Ca^{2+} content, a phenomenon that could presumably be beneficial in reducing the appearance of Ca^{2+} waves. This reduction in SR Ca^{2+} content was in fact evident when comparing the SR Ca^{2+} concentrations reached during selective SERCA stimulation with the Fab fragment of a PLB antibody with those reached during exposure to cAMP, which leads to RyR2 phosphorylation in addition to SERCA stimulation (Fig. 6.)
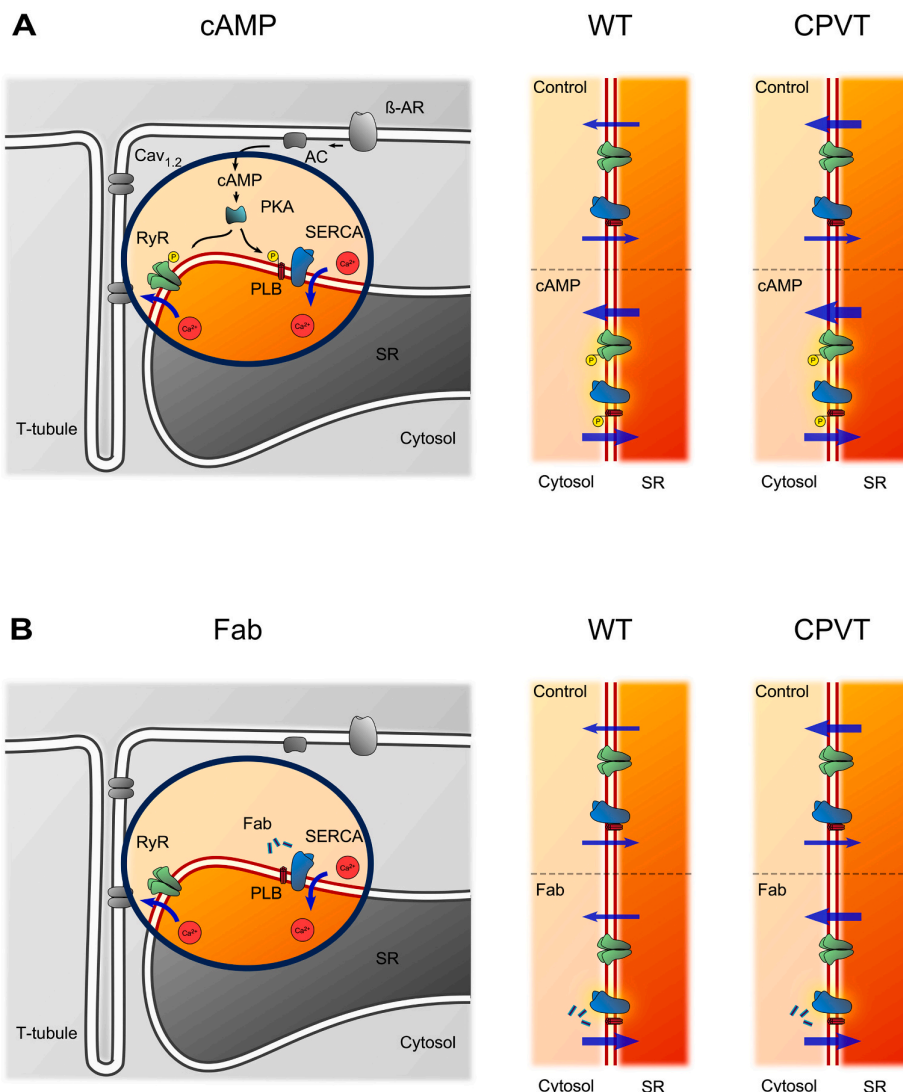

Fig. 8. Schematic representation of the changes in Ca^{2+} dynamics occurring in cardiomyocytes RyR2 activation and/or SERCA stimulation. Symbolic Ca^{2+} flux is represented by the arrow thickness connecting the cytosol and the SR. (A) In control conditions, the CPVT cells exhibit a slightly larger SR Ca^{2+} leak via RyRs than WT. Upon cAMP addition, both RyR2 and SERCA are stimulated. This results in enhanced SR Ca^{2+} uptake via SERCA and SR Ca^{2+} leak via RyR2, the latter is more pronounced in CPVT cells. Panel (B) shows the scenario during specific SERCA stimulation with the PLB antibody fragment Fab. While the SERCA activation is similar as in the presence of cAMP, the diastolic SR Ca^{2+} leak is initially not increasing. Overall, the absence of the enhanced leak leads to faster and more pronounced refilling of the SR with Ca^{2+}.

5. Conclusion

Based on these considerations, it appears conceivable that during ß-adrenergic stimulation, both mechanisms, the SERCA stimulation and the enhanced SR Ca^{2+} leak, can either contribute additively or negatively to the overall cellular arrhythmogenicity. Altogether, it is likely that the fine balance between the SR Ca^{2+} leak and Ca^{2+} uptake during the various conditions of physiological activity is a key determinant for the arrhythmogenicity phenotype found in the $RyR2^{R420Q+/-}$ mice. The same basic principle presumably applies to many, if not all, clinically relevant RyR2 mutations.

Data availability

All data used for the analysis will be made available through the public data repository Zenodo.org (DOI: https://doi.org/10.5281/zenodo.5226364).

Disclosures

The authors have declared that no conflict of interest exists.

Appendix A. Supplementary data

Supplementary data to this article can be found online at https://doi.org/10.1016/j.yjmcc.2022.05.011.

References

[1] D.M. Bers, Cardiac excitation-contraction coupling, Nature 415 (2002) 198–205, https://doi.org/10.1038/415198a.

[2] A. Leenhardt, I. Denjoy, P. Guicheney, Catecholaminergic polymorphic ventricular tachycardia, Circ. Arrhythm. Electrophysiol. 5 (2012) 1044–1052, https://doi.org/10.1161/CIRCEP.111.962027.

[3] A. Medeiros-Domingo, Z.A. Bhuiyan, D.J. Tester, N. Hofman, H. Bikker, J.P. van Tintelen, M.M. Mannens, A.A. Wilde, M.J. Ackerman, The *RYR2*-encoded ryanodine receptor/calcium release channel in patients diagnosed previously with either catecholaminergic polymorphic ventricular tachycardia or genotype negative, exercise-induced long QT syndrome: a comprehensive open reading frame mutational analysis, J. Am. Coll. Cardiol. 54 (2009) 2065–2074, https://doi.org/10.1016/j.jacc.2009.08.022.

[4] M. Fernandez-Velasco, A. Rueda, N. Rizzi, J.P. Benitah, B. Colombi, C. Napolitano, S.G. Priori, S. Richard, A.M. Gomez, Increased Ca^{2+} sensitivity of the ryanodine receptor mutant $RyR2^{R4496C}$ underlies catecholaminergic polymorphic ventricular tachycardia, Circ. Res. 104 (2009) 201–209, https://doi.org/10.1161/CIRCRESAHA.108.177493.

[5] D. Jiang, R. Wang, B. Xiao, H. Kong, D.J. Hunt, P. Choi, L. Zhang, S.R. Chen, Enhanced store overload-induced Ca^{2+} release and channel sensitivity to luminal Ca^{2+} activation are common defects of RyR2 mutations linked to ventricular tachycardia and sudden death, Circ. Res. 97 (2005) 1173–1181, https://doi.org/10.1161/01.RES.0000192146.85173.4b.

[6] D. Jiang, B. Xiao, L. Zhang, S.R. Chen, Enhanced basal activity of a cardiac Ca^{2+} release channel (ryanodine receptor) mutant associated with ventricular tachycardia and sudden death, Circ. Res. 91 (2002) 218–225, https://doi.org/10.1161/01.res.0000028455.36940.5e.

[7] Y.T. Zhao, C.R. Valdivia, G.B. Gurrola, P.P. Powers, B.C. Willis, R.L. Moss, J. Jalife, H.H. Valdivia, Arrhythmogenesis in a catecholaminergic polymorphic ventricular tachycardia mutation that depresses ryanodine receptor function, Proc. Natl. Acad.

Sci. U. S. A. 112 (2015) E1669–E1677, https://doi.org/10.1073/pnas.1419795112.

[8] T.M. Roston, W. Guo, A.D. Krahn, R. Wang, F. Van Petegem, S. Sanatani, S.R. Chen, A. Lehman, A novel *RYR2* loss-of-function mutation (I4855M) is associated with left ventricular non-compaction and atypical catecholaminergic polymorphic ventricular tachycardia, J. Electrocardiol. 50 (2017) 227–233, https://doi.org/10.1016/j.jelectrocard.2016.09.006.

[9] S.O. Marx, S. Reiken, Y. Hisamatsu, T. Jayaraman, D. Burkhoff, N. Rosemblit, A. R. Marks, PKA phosphorylation dissociates FKBP12.6 from the calcium release channel (ryanodine receptor): defective regulation in failing hearts, Cell 101 (2000) 365–376, https://doi.org/10.1016/s0092-8674(00)80847-8.

[10] S. Reiken, M. Gaburjakova, S. Guatimosim, A.M. Gomez, J. D'Armiento, D. Burkhoff, J. Wang, G. Vassort, W.J. Lederer, A.R. Marks, Protein kinase A phosphorylation of the cardiac calcium release channel (ryanodine receptor) in normal and failing hearts. Role of phosphatases and response to isoproterenol, J. Biol. Chem. 278 (2003) 444–453, https://doi.org/10.1074/jbc.M207028200.

[11] A.J. Lokuta, T.B. Rogers, W.J. Lederer, H.H. Valdivia, Modulation of cardiac ryanodine receptors of swine and rabbit by a phosphorylation-dephosphorylation mechanism, J. Physiol. 487 (1995) 609–622, https://doi.org/10.1113/jphysiol.1995.sp020904.

[12] W. Chen, R. Wang, B. Chen, X. Zhong, H. Kong, Y. Bai, Q. Zhou, C. Xie, J. Zhang, A. Guo, X. Tian, P.P. Jones, M.L. O'Mara, Y. Liu, T. Mi, L. Zhang, J. Bolstad, L. Semeniuk, H. Cheng, J. Zhang, J. Chen, D.P. Tieleman, A.M. Gillis, H.J. Duff, M. Fill, L.S. Song, S.R. Chen, The ryanodine receptor store-sensing gate controls Ca^{2+} waves and Ca^{2+}-triggered arrhythmias, Nat. Med. 20 (2014) 184–192, https://doi.org/10.1038/nm.3440.

[13] L. Yin, A. Zahradnikova Jr., R. Rizzetto, S. Boncompagni, C. Rabesahala de Meritens, Y. Zhang, P. Joanne, E. Marques-Sule, Y. Aguilar-Sanchez, M. Fernandez-Tenorio, O. Villejoubert, L. Li, Y.Y. Wang, P. Mateo, V. Nicolas, P. Gerbaud, F. A. Lai, R. Perrier, J.L. Alvarez, E. Niggli, H.H. Valdivia, C.R. Valdivia, J. Ramos-Franco, E. Zorio, S. Zissimopoulos, F. Protasi, J.P. Benitah, A.M. Gomez, Impaired binding to junctophilin-2 and nanostructural alteration in CPVT mutation, Circ. Res. 129 (2021) e35–e52, https://doi.org/10.1161/CIRCRESAHA.121.319094.

[14] Y.Y. Wang, P. Mesirca, E. Marques-Sule, A. Zahradnikova Jr., O. Villejoubert, P. D'Ocon, C. Ruiz, D. Domingo, E. Zorio, M.E. Mangoni, J.P. Benitah, A.M. Gomez, $RyR2^{R420Q}$ catecholaminergic polymorphic ventricular tachycardia mutation induces bradycardia by disturbing the coupled clock pacemaker mechanism, JCI Insight 2 (2017), https://doi.org/10.1172/jci.insight.91872 e91872.

[15] M. Fernandez-Tenorio, E. Niggli, Stabilization of Ca^{2+} signaling in cardiac muscle by stimulation of SERCA, J. Mol. Cell. Cardiol. 119 (2018) 87–95, https://doi.org/10.1016/j.yjmcc.2018.04.015.

[16] W.E. Louch, K.A. Sheehan, B.M. Wolska, Methods in cardiomyocyte isolation, culture, and gene transfer, J. Mol. Cell. Cardiol. 51 (2011) 288–298, https://doi.org/10.1016/j.yjmcc.2011.06.012.

[17] E. Bovo, S. Huke, L.A. Blatter, A.V. Zima, The effect of PKA-mediated phosphorylation of ryanodine receptor on SR Ca^{2+} leak in ventricular myocytes, J. Mol. Cell. Cardiol. 104 (2017) 9–16, https://doi.org/10.1016/j.yjmcc.2017.01.015.

[18] D.M. Potenza, R. Janicek, M. Fernandez-Tenorio, E. Camors, R. Ramos-Mondragon, H.H. Valdivia, E. Niggli, Phosphorylation of the ryanodine receptor 2 at serine 2030 is required for a complete ß-adrenergic response, J Gen Physiol 151 (2019) 131–145, https://doi.org/10.1085/jgp.201812155.

[19] Y.H. Chan, W.C. Tsai, Z. Song, C.Y. Ko, Z. Qu, J.N. Weiss, S.F. Lin, P.S. Chen, L. R. Jones, Z. Chen, Acute reversal of phospholamban inhibition facilitates the rhythmic whole-cell propagating calcium waves in isolated ventricular myocytes, J. Mol. Cell. Cardiol. 80 (2015) 126–135, https://doi.org/10.1016/j.yjmcc.2014.12.024.

[20] M. Fernandez-Tenorio, E. Niggli, Real-time intra-store confocal Ca^{2+} imaging in isolated mouse cardiomyocytes, Cell Calcium 60 (2016) 331–340, https://doi.org/10.1016/j.ceca.2016.07.002.

[21] E. Niggli, M. Fernandez-Tenorio, Simultaneous recording of subcellular Ca^{2+} signals from the cytosol and sarco/endoplasmic reticulum: compartmentalized dye loading, imaging, and analysis, Methods Mol. Biol. 2019 (1929) 53–71, https://doi.org/10.1007/978-1-4939-9030-6_5.

[22] E.A. Sobie, L.S. Song, W.J. Lederer, Local recovery of Ca^{2+} release in rat ventricular myocytes, J. Physiol. 565 (2005) 441–447, https://doi.org/10.1113/jphysiol.2005.086496.

[23] E. Polakova, A. Illaste, E. Niggli, E.A. Sobie, Maximal acceleration of Ca^{2+} release refractoriness by β-adrenergic stimulation requires dual activation of kinases PKA and CaMKII in mouse ventricular myocytes, J. Physiol. 593 (2015) 1495–1507, https://doi.org/10.1113/jphysiol.2014.278051.

[24] S.J. Lord, K.B. Velle, R.D. Mullins, L.K. Fritz-Laylin, SuperPlots: communicating reproducibility and variability in cell biology, J. Cell Biol. 219 (2020), https://doi.org/10.1083/jcb.202001064 e202001064.

[25] M.B. Sikkel, D.P. Francis, J. Howard, F. Gordon, C. Rowlands, N.S. Peters, A. R. Lyon, S.E. Harding, K.T. MacLeod, Hierarchical statistical techniques are necessary to draw reliable conclusions from analysis of isolated cardiomyocyte studies, Cardiovasc. Res. 113 (2017) 1743–1752, https://doi.org/10.1093/cvr/cvx151.

[26] S.E. Lehnart, X.H. Wehrens, P.J. Laitinen, S.R. Reiken, S.X. Deng, Z. Cheng, D. W. Landry, K. Kontula, H. Swan, A.R. Marks, Sudden death in familial polymorphic ventricular tachycardia associated with calcium release channel (ryanodine receptor) leak, Circulation 109 (2004) 3208–3214, https://doi.org/10.1161/01.CIR.0000132472.98675.EC.

[27] S.C. Salvage, E.M. Gallant, N.A. Beard, S. Ahmad, H. Valli, J.A. Fraser, C.L. Huang, A.F. Dulhunty, Ion channel gating in cardiac ryanodine receptors from the

arrhythmic RyR2-P2328S mouse, J. Cell. Sci. 132 (2019), https://doi.org/10.1242/jcs.229039 jcs229039.

[28] H.R. Ramay, O.Z. Liu, E.A. Sobie, Recovery of cardiac calcium release is controlled by sarcoplasmic reticulum refilling and ryanodine receptor sensitivity, Cardiovasc. Res. 91 (2011) 598–605, https://doi.org/10.1093/cvr/cvr143.

[29] R. Janicek, H. Agarwal, A.M. Gomez, M. Egger, G.C.R. Ellis-Davies, E. Niggli, Local recovery of cardiac calcium-induced calcium release interrogated by ultra-effective, two-photon uncaging of calcium, J. Physiol. 599 (2021) 3841–3852, https://doi.org/10.1113/JP281482.

[30] A.M. Gomez, H. Cheng, W.J. Lederer, D.M. Bers, Ca^{2+} diffusion and sarcoplasmic reticulum transport both contribute to $[Ca^{2+}]_i$ decline during Ca^{2+} sparks in rat ventricular myocytes, J. Physiol. 496 (Pt 2) (1996) 575–581, https://doi.org/10.1113/jphysiol.1996.sp021708.

[31] D.R. Witcher, R.J. Kovacs, H. Schulman, D.C. Cefali, L.R. Jones, Unique phosphorylation site on the cardiac ryanodine receptor regulates calcium channel activity, J. Biol. Chem. 266 (1991) 11144–11152. https://www.ncbi.nlm.nih.gov/pubmed/1645727.

[32] B. Xiao, M.T. Jiang, M. Zhao, D. Yang, C. Sutherland, F.A. Lai, M.P. Walsh, D.C. Warltier, H. Cheng, S.R. Chen, Characterization of a novel PKA phosphorylation site, serine-2030, that regulates the cardiac ryanodine receptor in canine heart failure, Circ. Res. 96 (2005) 847–855, https://doi.org/10.1161/01.RES.0000163276.26083.e8.

[33] P.P. Jones, X. Meng, B. Xiao, S. Cai, J. Bolstad, T. Wagenknecht, Z. Liu, S.R. Chen, Localization of PKA phosphorylation site, Ser^{2030}, in the three-dimensional structure of cardiac ryanodine receptor, Biochem. J. 410 (2008) 261–270, https://doi.org/10.1042/BJ20071257.

[34] H.H. Valdivia, J.H. Kaplan, G.C. Ellis-Davies, W.J. Lederer, Rapid adaptation of cardiac ryanodine receptors: modulation by Mg^{2+} and phosphorylation, Science 267 (1995) 1997–2000, https://doi.org/10.1126/science.7701323.

[35] V. Bauerova-Hlinkova, D. Hajduchova, J.A. Bauer, Structure and function of the human ryanodine receptors and their association with myopathies-present state, challenges, and perspectives, Molecules 25 (2020) 4040, https://doi.org/10.3390/molecules25184040.

[36] W. Guo, J. Wei, J.P. Estillore, L. Zhang, R. Wang, B. Sun, S.R.W. Chen, RyR2 disease mutations at the C-terminal domain intersubunit interface alter closed-state stability and channel activation, J. Biol. Chem. 297 (2021), https://doi.org/10.1016/j.jbc.2021.100808, 100808.

[37] D. Domingo, P. Neco, E. Fernandez-Pons, S. Zissimopoulos, P. Molina, J. Olague, M.P. Suarez-Mier, F.A. Lai, A.M. Gomez, E. Zorio, Non-ventricular, clinical, and functional features of the $RyR2^{R420Q}$ mutation causing catecholaminergic polymorphic ventricular tachycardia, Rev. Esp. Cardiol. (Engl. Ed.) 68 (2015) 398–407, https://doi.org/10.1016/j.rec.2014.04.023.

[38] X.H. Zhang, H. Wei, Y. Xia, M. Morad, Calcium signaling consequences of RyR2 mutations associated with CPVT1 introduced via CRISPR/Cas9 gene editing in human-induced pluripotent stem cell-derived cardiomyocytes: comparison of RyR2-R420Q, F2483I, and Q4201R, Heart Rhythm. 18 (2021) 250–260, https://doi.org/10.1016/j.hrthm.2020.09.007.

[39] K.A. Iyer, Y. Hu, A.R. Nayak, N. Kurebayashi, T. Murayama, M. Samso, Structural mechanism of two gain-of-function cardiac and skeletal RyR mutations at an equivalent site by cryo-EM, Sci. Adv. 6 (2020), https://doi.org/10.1126/sciadv.abb2964 eabb2964.

[40] B. Xiao, G. Zhong, M. Obayashi, D. Yang, K. Chen, M.P. Walsh, Y. Shimoni, H. Cheng, H. Ter Keurs, S.R. Chen, Ser-2030, but not Ser-2808, is the major phosphorylation site in cardiac ryanodine receptors responding to protein kinase A activation upon β-adrenergic stimulation in normal and failing hearts, Biochem. J. 396 (2006) 7–16, https://doi.org/10.1042/BJ20060116.

[41] X.H. Wehrens, S.E. Lehnart, S.R. Reiken, A.R. Marks, Ca^{2+}/calmodulin-dependent protein kinase II phosphorylation regulates the cardiac ryanodine receptor, Circ. Res. 94 (2004) e61–e70, https://doi.org/10.1161/01.RES.0000125626.33738.E2.

[42] S. Gyorke, I. Gyorke, V. Lukyanenko, D. Terentyev, S. Viatchenko-Karpinski, T.F. Wiesner, Regulation of sarcoplasmic reticulum calcium release by luminal calcium in cardiac muscle, Front. Biosci. 7 (2002) d1454–d1463. https://www.ncbi.nlm.nih.gov/pubmed/12045014.

[43] V. Lukyanenko, S. Viatchenko-Karpinski, A. Smirnov, T.F. Wiesner, S. Gyorke, Dynamic regulation of sarcoplasmic reticulum Ca^{2+} content and release by luminal Ca^{2+}-sensitive leak in rat ventricular myocytes, Biophys. J. 81 (2001) 785–798, https://doi.org/10.1016/S0006-3495(01)75741-4.

[44] V. Lukyanenko, S. Subramanian, I. Gyorke, T.F. Wiesner, S. Gyorke, The role of luminal Ca^{2+} in the generation of Ca^{2+} waves in rat ventricular myocytes, J. Physiol. 518 (1999) 173–186, https://doi.org/10.1111/j.1469-7793.1999.0173r.x.

[45] P.P. Jones, W. Guo, S.R.W. Chen, Control of cardiac ryanodine receptor by sarcoplasmic reticulum luminal Ca^{2+}, J. Gen. Physiol. 149 (2017) 867–875, https://doi.org/10.1085/jgp.201711805.

[46] D. Jiang, W. Chen, R. Wang, L. Zhang, S.R. Chen, Loss of luminal Ca^{2+} activation in the cardiac ryanodine receptor is associated with ventricular fibrillation and sudden death, Proc. Natl. Acad. Sci. U. S. A. 104 (2007) 18309–18314, https://doi.org/10.1073/pnas.0706573104.

[47] Y. Bai, P.P. Jones, J. Guo, X. Zhong, R.B. Clark, Q. Zhou, R. Wang, A. Vallmitjana, R. Benitez, L. Hove-Madsen, L. Semeniuk, A. Guo, L.S. Song, H.J. Duff, S.R. Chen, Phospholamban knockout breaks arrhythmogenic Ca^{2+} waves and suppresses catecholaminergic polymorphic ventricular tachycardia in mice, Circ. Res. 113 (2013) 517–526, https://doi.org/10.1161/CIRCRESAHA.113.301678.

[48] D. Sato, H. Uchinoumi, D.M. Bers, Increasing SERCA function promotes initiation of calcium sparks and breakup of calcium waves, J. Physiol. 599 (2021) 3267–3278, https://doi.org/10.1113/JP281579.

[49] A. Kalyanasundaram, V.A. Lacombe, A.E. Belevych, L. Brunello, C.A. Carnes, P.M. Janssen, B.C. Knollmann, M. Periasamy, S. Gyorke, Up-regulation of sarcoplasmic reticulum Ca^{2+} uptake leads to cardiac hypertrophy, contractile dysfunction and early mortality in mice deficient in CASQ2, Cardiovasc. Res. 98 (2013) 297–306, https://doi.org/10.1093/cvr/cvs334.